Charge Fractionalization in the Integer Quantum Hall Effect

Hiroyuki Inoue,[1] Anna Grivnin,[1] Nissim Ofek,[2] Izhar Neder,[3] Moty Heiblum,[1] Vladimir Umansky,[1] and Diana Mahalu[1]

[1]*Braun Center for Submicron Research, Department of Condensed Matter Physics, Weizmann Institute of Science, 79100 Rehovot, Israel*

[2]*Departments of Physics and Applied Physics, Yale University, New Haven, Connecticut 06520, USA*

[3]*Raymond and Beverly Sackler School of Physics and Astronomy, Tel-Aviv University, 69978 Tel Aviv, Israel*

(Received 14 January 2014; published 25 April 2014; corrected 29 April 2014)

We report an observation, via sensitive shot noise measurements, of charge fractionalization of chiral edge electrons in the integer quantum Hall effect regime. Such fractionalization results solely from interchannel Coulomb interaction, leading electrons to decompose to excitations carrying fractional charges. The experiment was performed by guiding a partitioned current carrying edge channel in proximity to another unbiased edge channel, leading to shot noise in the unbiased edge channel without net current, which exhibited an unconventional dependence on the partitioning. The determination of the fractional excitations, as well as the relative velocities of the two original (prior to the interaction) channels, relied on a recent theory pertaining to this measurement. Our result exemplifies the correlated nature of multiple chiral edge channels in the integer quantum Hall effect regime.

DOI: 10.1103/PhysRevLett.112.166801 PACS numbers: 73.43.Lp, 42.50.Lc

Charge fractionalization is an emergent phenomenon in low-dimensional correlated electrons. A known example is that of fractional charges in the fractional quantum Hall regime, which is a consequence of strong Coulomb interaction among two-dimensional electrons in partially filled Landau levels [1–6], as well as fractionalization in one-dimensional quantum wires [7–9]. On the contrary, the integer quantum Hall effect (IQHE), with electrons behaving largely as independent particles, lacks such intrinsic fractionalization.

Transport in the IQHE regime takes place solely at sample's periphery via gapless chiral edge channels [10,11]. Spatial separation between the channels allows manipulating each channel individually; customarily with a quantum point contact (QPC) constriction. Counter propagating (upstream) neutral edge modes in fractional quantum Hall states revealed the importance of interchannel Coulomb interaction accompanied by interchannel tunneling due to impurities [12–15]. On the other hand, while interaction between electrons is usually ignored in the IQHE regime, there is plenty of evidence to support its existence, including the following observations: (i) "lobe structures" in the visibility of edge channel interferometers—attributed to electron interaction [16–21], (ii) interaction-mediated dephasing [18,20–23], and (iii) energy relaxation of nonequilibrium electrons among adjacent edge channels [24–27].

Interchannel interaction can be monitored in a direct fashion. In $\nu = 2$, Coulomb interaction between electrons in the two adjacent edge channels is expected to modify the noninteracting channels [19,20,28–33]. An electron injected selectively into the "hot" channel, while the other channel is "cold," is predicted to decompose into two modes—"fast" and "slow." Each is shared between the two original channels, and each carries a fraction of an electron charge [28–34]. Indeed, a recent rf transmission measurement investigated the detailed dispersion of the slow mode and its separation from the fast mode [34]. Our approach was to partition the cold channel after it had interacted with the partitioned hot one, with a resulted low-frequency shot noise in the cold channel (with zero net current). The fractional charges and the relative velocities of the two original channels were then determined from the shot noise [33], elucidating and quantifying the fractionalization phenomenon.

It might be illuminating to present first an intuitive model of our experimental system, with electrons injected into the hot channel [channel 1, partitioned by QPC1, in Fig. 1(a)]. The resulting excitations in the two channels (1 and 2) can be regarded as fractionally charged dipoles flowing downstream, with the spin degree of freedom playing no role. Assuming short range interchannel interaction $uh\delta(x_1 - x_2)$, the energy density of the interacting channels is $\varepsilon = h(v_1\rho_1^2 + v_2\rho_2^2 + u\rho_1\rho_2)$ where h is Planck's constant, $\rho_1(x_1)$ and $\rho_2(x_2)$ are the number densities, and v_1, v_2 are the velocities of the bare channels. Diagonalizing the velocity matrix $\left(\begin{smallmatrix} v_1 & u/2 \\ u/2 & v_2 \end{smallmatrix}\right)$ with one electron injected into channel 1, the eigenmodes are (i) the slow mode, consisting of a particlelike charge $+(1-\alpha)e$ and a holelike charge $-\beta e$ and (ii) the fast mode, consisting of particlelike charges $+\alpha e$ and $+\beta e$. Here, $\alpha = (1+\cos\theta)/2$, $\beta = (\sin\theta)/2$, and $\tan\theta = u/\Delta v$ $(0 < \theta < \pi/2)$, with θ the so-called mixing angle, and $\Delta v = v_1 - v_2$. The two modes propagate at velocities $v_\pm = \bar{v} \pm \frac{1}{2}\sqrt{(\Delta v)^2 + u^2}$, where $\bar{v} = (v_1 + v_2)/2$ and

+ (−) stands for "fast" ("slow"). Noting that for $\Delta v = 0$, $\alpha = \beta = 1/2$ and the slow mode is neutral. Moreover, $4v_1v_2 > u^2$ must be satisfied for the stability ($v_- > 0$). Evidently, the cold channel always carries zero net current with a fluctuating neutral excitation, $+\beta e$ and $-\beta e$. Partitioning the cold channel stochastically (with QPC2) is expected to generate white shot noise, which can be measured through its zero-frequency spectral density S_i.

Our device was fabricated in a GaAs/AlGaAs heterostructure embedding 2DEG, 130 nm below the surface, whose density is 8.2×10^{10} cm^{-2} and dark mobility 4.2×10^6 cm^2/Vs at 4.2 K [Fig. 1(b)]. The light blue region is a mesa; the light gray curves are metallic gates (5 nmTi/15 nmAu) forming the QPCs (600 nm opening) and a side gate (SG, placed off the mesa and kept at $V_{SG} = -500$ mV); the yellow pads are alloyed AuGeNi Ohmic contacts. Source contacts are S1 and S2 (driving current $2I$; I per channel), G grounds, and A1, A2 amplifier contacts (each loaded with a resonant circuit, $f_0 \sim 790$ kHz, followed by a homemade cryogenic preamplifier). Measurements were performed at a magnetic field $B = 1.7$ T, around the center of the $\nu = 2$ plateau. Having a relatively low magnetic field, we assured the absence of edge reconstructions, which modify the electron density profile perpendicular to the edge, possibly adding extra edge channels, and the presence of only two electron channels at the edge [35]. The expected shot noise due to stochastic partitioning (transmission probability T) is $S_i = 2eIT(1-T)(\coth x - x^{-1})$, with $x = eI/2k_B\Theta G_0$, with $k_B\Theta$ the thermal energy ($\Theta \sim 20$ mK in our system) and $G_0 = e^2/h$ [36]. The interaction region, defined by the two QPCs, is $l = 8$ μm, being nearly the distance needed for energy equilibration [24]. We have also tested a device with $l = 40$ μm, which included an added gate that allowed us to control the spatial separation between the two channels [37].

While a few theories had considered our experimental scheme [31–33], Ref. [33] computed the fractionalization noise as a function of T_1 and up to the linear order in $R_2 = 1 - T_2$, and thus provided (i) a relation between the mixing angle θ and a Fano factor [see Fig. 2(a)] and (ii) an expression for the dependence of the shot noise on T_1, namely $[T_1(1-T_1)]^{\gamma_1}$. The Fano factor $F(\theta) = S_i/S_{ref}$, where $S_{ref} = 4eIT_1(1-T_1)R_2$ with $R_2 << 1$, reflects the fractional charge in the cold channel, $e^* = Fe$, only for $T_1 \cong 0.5$. Here, S_{ref} is the expected excess noise due to stochastic weak backscattering of a random train of electrons and holes. In general, $F(\theta) \propto [T_1(1-T_1)]^{\gamma_1 - 1}$ is T_1 dependent; however, as shown in Fig. 2(a), $F(\theta)$ for $T_1 \cong 0.5$ (solid curve) indeed resembles the charge $\beta = (\sin\theta)/2$ (dotted curve); hence, $F \sim \beta$. Assuming a steady state without dissipation to external environment, the

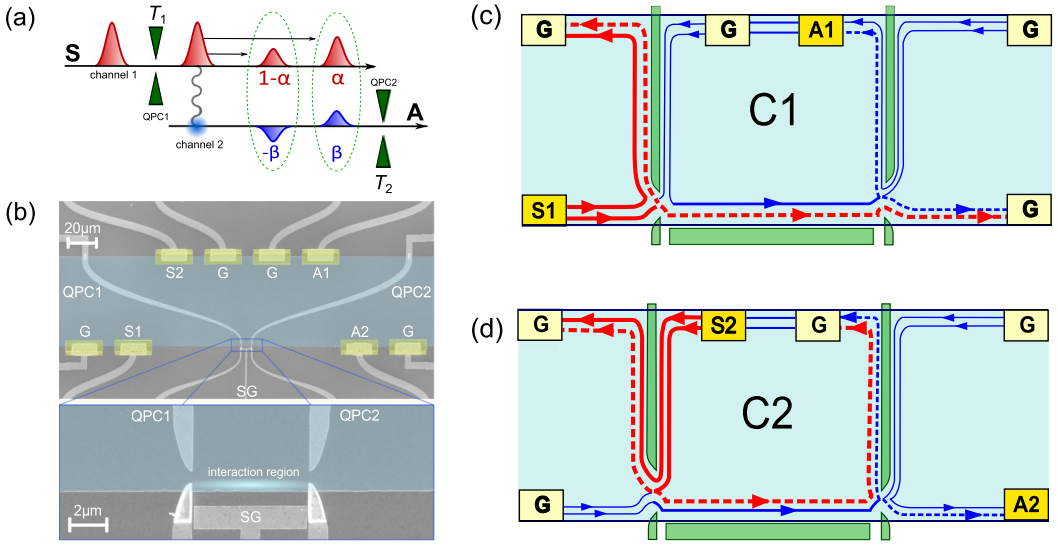

FIG. 1 (color online). (a) An ordered train of electrons driven from the source (S) transmit the QPC1 with a probability T_1 and decompose into fast and slow modes. The fast mode consists of fractional charges $\alpha e(\beta e)$ on channel 1 (2) and the slow mode consists of fractional charges $(1-\alpha)e$, $(-\beta e)$ on channel 1 (2). The pairs of $\pm\beta e$ are partitioned at QPC2 with a transmission probability T_2, generating a low-frequency shot noise to be detected at the amplifier (A). (b) A SEM image of the employed device. Below, a magnified view of the core part. The region between the QPCs is the interaction region ($l = 8$ μm). (c) Configuration 1 ($C1$). S1 and A1 were employed. The red and the blue arrows are the hot and cold channels. The biased outer channel is the channel 1 (hot channel) here. QPC1 fully reflects the inner channel while partitions the outer channel (dotted heavy red line). Two cold edge channels, emanating from the G contacts, also impinge at QPC1 (thin blue lines), where the outer is fully transmitted and the inner fully reflected. The reflected cold channel (thick blue line) flows in close proximity to the partitioned outer channel, with both reaching QPC2. There, the outer channel is fully transmitted and inner one is being partitioned by half (dotted thick blue line), with its excess current noise (spectral density, S_i) monitored at A1. (d) Configuration 2 ($C2$). S2 and A2 were employed. The biased inner channel is the hot channel here. T_1 was set to half-transmitting for the inner channel and the reflected part was directed to QPC2 with various T_2 to partition the fluctuating cold outer channel.

coefficient γ_1 was calculated to span $0.68 \leq \gamma_1(\theta) \leq 1$ with $0 < \theta < \pi/2$ [33]. Measuring $\gamma_1(\theta) = 0.68$ leads to $\theta = \pi/2$ and consequently to $\Delta v = 0$ and $\beta = \alpha = 0.5$. Approaching the noninteracting case, $\theta \to 0$, the noise in the cold channel diminishes, $F \to 0$ and $\gamma_1 \to 1$. Therefore, there are two ways to extract the fractional charge: (i) evaluating the Fano factor of the observed noise at $T_1 \cong 0.5$ and $R_2 \ll 1$ and (ii) finding γ_1 from the noise at various T_1, yielding θ, and thus $F(\theta)$ accordingly. If the results of the two methods coincide, our estimate of the fractional charge is likely to be reliable.

Two kinds of configurations were employed: $C1$ for T_1 dependence [Fig. 1(c)], and $C2$ for T_2 dependence [Fig. 1(d)], so that the two configurations were designated so that the variable transmission QPC was always in the outer channel, since it has a weaker energy dependence [namely, hot (cold) channel in $C1$ ($C2$)]. Note that tests were also performed when the roles of the channels were not reversed, leading to qualitatively similar results.

We start with testing the dependence of the excess noise S_i in A1 on T_1 in the configuration $C1$, keeping $T_2 = 0.5$ [Fig. 3(a)]. As the injected current $|I|$ in the hot channel increased, the excess noise in the cold channel also increased (resembling the ubiquitous "V" shape), but without the net current reaching A1. The normalized excess noise (with respect to that at $T_1 \cong 0.5$) is shown in Fig. 3(b), obeying dependence $[T_1(1-T_1)]^{\gamma_1}$ with $\gamma_1 = 0.71 \pm 0.08$. The error bars are 2σ, with σ the best-fit error, being limited by the $\sim$1 h integration time. Being a Gaussian noise, errors can be easily reduced by longer integration times (as was proven in numerous occasions). With errors of 1.2σ, we find $\gamma_1 = 0.71 \pm 0.01$.

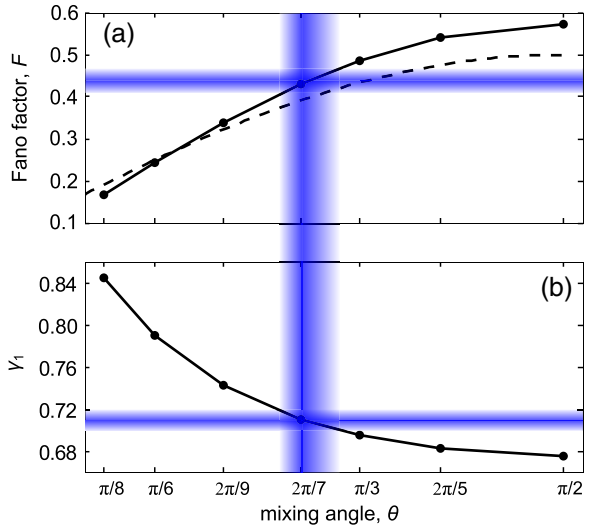

FIG. 2 (color online). (a) Reproduced figure of Ref. [33]. The Fano factor $F = S_i/S_{ref}$ ($S_{ref} = 4eIT_1R_1R_2$ with $R_2 \to 0$) representing the fractional charge in the cold channel ($e^* = Fe$), plotted as function of the mixing angle. The black dots are values evaluated by the theory ($T_1 = 0.5$, $R_2 \ll 1$) and the solid curve depicts $\beta = (\sin\theta)/2$ based on the simple model in the present paper. (b) The exponent γ_1 plotted as function of the mixing angle θ based on the numerical computation. The experimentally obtained $\gamma_1 = 0.71 \pm 0.01$ yields $\theta = \pi/3.2$–$\pi/3.7$, the ratio $u/\Delta v = 1.1$–1.5, and a Fano factor $F = 0.41$–0.46. Applying it to the simple model, are $\beta = 0.38$–0.41 and $\alpha = 0.78$–0.83. The blue blurred lines represents the best fit with the error of 1.2σ based on obtained exponent γ_1.

Similar measurements were repeated with configuration $C2$. The dependence of S_i in A2 on I and T_2 of the cold channel ($T_1 = 0.5$) is plotted in Fig. 4(a). In the same manner, a dependence $[T_2(1-T_2)]^{\gamma_2}$ of S_i was found [Fig. 4(b)] with $\gamma_2 = 0.97 \pm 0.02$ with an error of 1.2σ. Here, partitioning T_2 appears to be nearly binomial.

First, the nearly binomial dependence of the excess noise in T_2, $S_i \propto R_2(1-R_2)$ for $T_1 = 0.5$, is reduced to $S_i \propto R_2$ in the limit of $R_2 \to 0$, coinciding with the perturbative treatment in R_2 [33]. The merely independent (binomial) scattering events due to T_2 validate the extraction of γ_1 at $T_2 = 0.5$ (rather than $R_2 \ll 1$). Hence, we

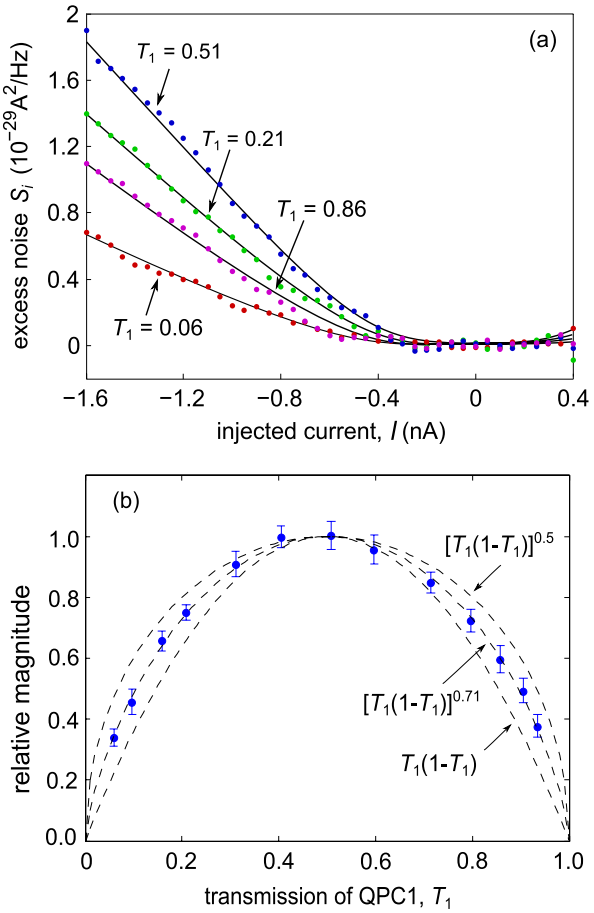

FIG. 3 (color online). (a) The excess noise traces (in $C1$) as a function of I for various T_1 with fixed $T_2 = 0.5$ and selected traces are shown. (b) Relative magnitude of the excess noise as a function of T_1, normalized to the one at $T_1 = 0.5$. The excess noise is proportional to $[T_1(1-T_1)]^{\gamma_1}$, where $\gamma_1 = 0.71 \pm 0.08$ with the error of 2σ, which reduces to $\gamma_1 = 0.71 \pm 0.01$ for 1.2σ. Curves with $\gamma_1 = 0.5$ and 1.0 are also plotted.

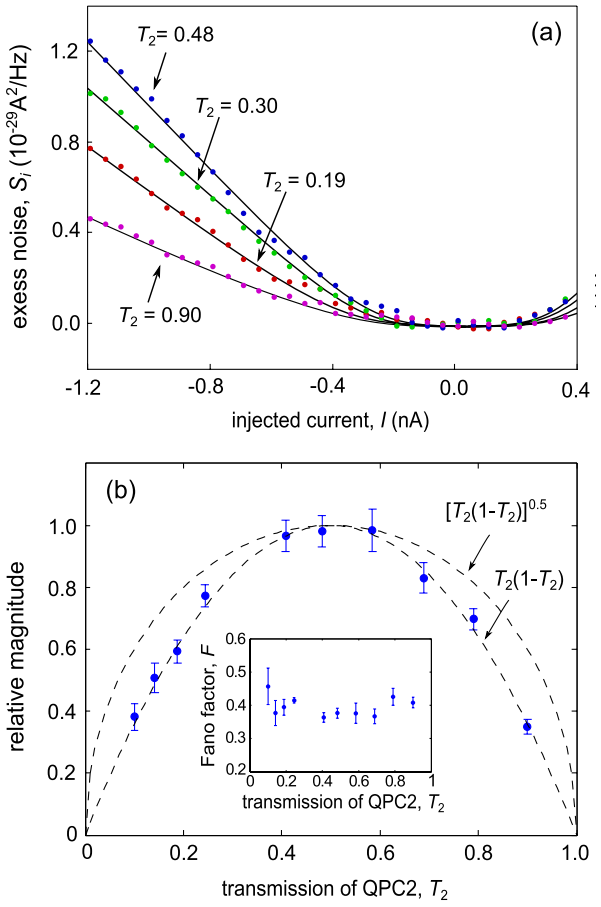

FIG. 4 (color online). (a) The excess noise traces (in $C2$) as a function of I for selected T_2 (with $T_1 = 0.5$) are shown. The linear part of the trace of $T_2 = 0.90$ was exploited to extract the Fano factor $F = 0.38 \pm 0.02$. (b) Relative magnitude of the excess noise as a function of T_2, normalized to the one at $T_2 = 0.5$, is plotted. The excess noise is proportional to $[T_1(1-T_1)]^{\gamma_1}$, where $\gamma_2 = 0.97 \pm 0.02$ for the error of 1.2σ. A dashed curve with $\gamma_2 = 0.5$ is plotted. The inset depicts the Fano factor evaluated with the extended reference noise $S_{ref} = 4eT_1R_1T_2R_2$ at all the employed T_2.

examined the relevance of an extended reference noise $S_{ref} = 4eT_1R_1T_2R_2$ by evaluating the Fano factor at various T_2 ($T_1 = 0.5$) and found an overall average 0.39 ± 0.03, [inset of Fig. 4(b)] making the extended reference noise plausible. Further theoretical considerations of T_2 dependence are necessary to verify this point.

Comparing our data with Ref. [33], we find that $\gamma_1 = 0.70$–0.72 falls within the predicted range of γ_1. The observed γ_1 leads to a mixing angle $\theta = \pi/3.7$–$\pi/3.2$, the ratio $u/\Delta v = 1.1$–1.5, and a Fano factor $F = 0.41$–0.46 (Fig. 2 and Ref. [33]). Moreover, the theoretical prediction was compared with our measured $F = 0.38 \pm 0.02$ (namely, the slope of the excess noise vs current in the range -1.2 nA $\leq I \leq -0.6$ nA, with $T_1 = 0.5$, $R_2 = 0.1$, divided by $4eT_1R_1R_2$), leading to an excellent agreement. With the obtained mixing angle, the fractional charges are $\beta = 0.38$–0.41 and $\alpha = 0.78$–0.83. The dissipation is a subtle issue. There are conflicting results from different methods in terms of the dissipations [24,34]. Our diagnostic on the degree of the dissipation is only comparing the Fano factor obtained two ways. Having obtained similar values for the Fano factor, we believe our system reached its steady state and experienced a negligible amount of dissipation [37].

In order to obtain u or Δv (having $u/\Delta v$), we exploit results from a similar configuration already reported in Ref. [22]. There an applied dc bias of 19 μV to the inner channel at $\nu = 2$ resulted in an addition of a single electron in a 10 μm long interaction length, leading to an estimated interchannel mutual capacitance $C = 0.84$ fF/μm. From it, $u = e^2/hC = 4.6 \times 10^4$ m/s, $\Delta v = 3.1 - 4.2 \times 10^4$ m/s, and the minimum $\bar{v} = 2.8 - 3.1 \times 10^4$ m/s (based on $v_- = 0$). The logarithmic dependent Coulomb interaction between the two channels makes the exact capacitance less important.

An intuitive picture of the mechanism that leads to excess shot noise with zero net current is as follows: The shot noise in the partitioned hot channel has a white spectrum with a frequency cutoff I/e. The interchannel capacitance $Cl = e^2 l/hu$ couples high-frequency components in the cold channel, acting as a high-pass filter with a low-frequency cutoff $\sim Cl/G_0$ (much higher than our measurement frequency). Therefore, the power spectrum of the cold channel (heading QPC2) exhibits a peak at a frequency related to $f^{-1} = l(v_-^{-1} - v_+^{-1})$. However, stochastic partitioning of that spectrum by QPC2 redistributes the high-frequency spectrum over the entire spectrum (up to the cutoff frequency),yet with zero net current (since, there is no electron tunneling into this channel). In other words, QPC2 stochastically breaks the pairs of $+\beta e$ and $-\beta e$ apart, leading to a wideband noise spectrum.

In summary, measuring weak signals of currentless shot noise allowed observation of charge fractionalization in a nonequilibrium, interacting edge channel in the IQHE regime (in $\nu = 2$), as well as the relative channels' velocity. Our scheme can be extended to various interacting one-dimensional systems such as topological surface and edge states and ultracold atoms to probe the correlation and relaxation physics.

We thank B. Rosenow, M. Milletarì, Y. Oreg, and G. Viola for helpful discussions and H. K. Choi for his technical help. We acknowledge the partial support of the Israeli Science Foundation (ISF), the Minerva Foundation, the U.S.-Israel Bi-National Science Foundation (BSF), and the European Research Council under the European Community's Seventh Framework Program (FP7/2007-2013)/ERC, Grant Agreement No. 227716.

Note added in proof.—During the writing of this manuscript we became aware of a work aiming similarly in which the authors observed fractionalized wave packets in pulsed measurements [38].

[1] R. B. Laughlin, Phys. Rev. Lett. **50**, 1395 (1983).
[2] X. G. Wen, Phys. Rev. B **41**, 12838 (1990).
[3] R. de-Picciotto, M. Reznikov, M. Heiblum, V. Umansky, G. Bunin, and D. Mahalu, Nature (London) **389**, 162 (1997).
[4] L. Saminadayar, D. C. Glattli, Y. Jin, and B. Etienne, Phys. Rev. Lett. **79**, 2526 (1997).
[5] J. Martin, S. Ilani, B. Verdene, J. Smet, V. Umansky, D. Mahalu, D. Schuh, G. Abstreiter, and A. Yacoby, Science **305**, 980 (2004).
[6] N. Ofek, A. Bid, M. Heiblum, A. Stern, V. Umansky, and D. Mahalu, Proc. Natl. Acad. Sci. U.S.A. **107**, 5276 (2010).
[7] I. Safi and H. J. Schulz, Phys. Rev. B **52**, R17040 (1995).
[8] K.-V. Pham, M. Gabay, and P. Lederer, Phys. Rev. B **61**, 16397 (2000).
[9] H. Steinberg, G. Barak, A. Yacoby, L. N. Pfeiffer, K. W. West, B. I. Halperin, and K. Le Hur, Nat. Phys. **4**, 116 (2007).
[10] B. I. Halperin, Phys. Rev. B **25**, 2185 (1982).
[11] M. Büttiker, Phys. Rev. B **38**, 9375 (1988).
[12] C. Kane, M. Fisher, and J. Polchinski, Phys. Rev. Lett. **72**, 4129 (1994).
[13] C. L. Kane and M. P. A. Fisher, Phys. Rev. B **51**, 13449 (1995).
[14] A. Bid, N. Ofek, H. Inoue, M. Heiblum, C. L. Kane, V. Umansky, and D. Mahalu, Nature (London) **466**, 585 (2010).
[15] H. Inoue, A. Grivnin, Y. Ronen, M. Heiblum, V. Umansky, and D. Mahalu, arXiv:1312.7553.
[16] I. Neder, M. Heiblum, Y. Levinson, D. Mahalu, and V. Umansky, Phys. Rev. Lett. **96**, 016804 (2006).
[17] P. Roulleau, F. Portier, D. C. Glattli, P. Roche, A. Cavanna, G. Faini, U. Gennser, and D. Mailly, Phys. Rev. B **76**, 161309 (2007).
[18] F. Marquardt, Phys. Rev. B **74**, 125319 (2006).
[19] J. T. Chalker, Y. Gefen, and M. Y. Veillette, Phys. Rev. B **76**, 085320 (2007).
[20] I. P. Levkivskyi and E. V. Sukhorukov, Phys. Rev. B **78**, 045322 (2008).
[21] C. Neuenhahn and F. Marquardt, New J. Phys. **10**, 115018 (2008).
[22] I. Neder, F. Marquardt, M. Heiblum, D. Mahalu, and V. Umansky, Nat. Phys. **3**, 534 (2007).
[23] P. Roulleau, F. Portier, P. Roche, A. Cavanna, G. Faini, U. Gennser, and D. Mailly, Phys. Rev. Lett. **101**, 186803 (2008).
[24] H. le Sueur, C. Altimiras, U. Gennser, A. Cavanna, D. Mailly, and F. Pierre, Phys. Rev. Lett. **105**, 056803 (2010).
[25] P. Degiovanni, C. Grenier, G. Fève, C. Altimiras, H. le Sueur, and F. Pierre, Phys. Rev. B **81**, 121302 (2010).
[26] A. M. Lunde, S. E. Nigg, and M. Büttiker, Phys. Rev. B **81**, 041311 (2010).
[27] I. P. Levkivskyi and E. V. Sukhorukov, Phys. Rev. B **85**, 075309 (2012).
[28] E. Berg, Y. Oreg, E.-A. Kim, and F. von Oppen, Phys. Rev. Lett. **102**, 236402 (2009).
[29] J. M. Leinaas, M. Horsdal, and T. H. Hansson, Phys. Rev. B **80**, 115327 (2009).
[30] M. Horsdal, M. Rypestøl, H. Hansson, and J. M. Leinaas, Phys. Rev. B **84**, 115313 (2011).
[31] I. Neder, Phys. Rev. Lett. **108**, 186404 (2012).
[32] I. P. Levkivskyi and E. V. Sukhorukov, Phys. Rev. Lett. **109**, 246806 (2012).
[33] M. Milletarì and B. Rosenow, Phys. Rev. Lett. **111**, 136807 (2013).
[34] E. Bocquillon, V. Freulon, J.-M. Berroir, P. Degiovanni, B. Plaçais, A. Cavanna, Y. Jin, and G. Fève, Nat. Commun. **4**, 1839 (2013).
[35] V. Venkatachalam, S. Hart, L. Pfeiffer, K. West, and A. Yacoby, Nat. Phys. **8**, 676 (2012).
[36] T. Martin and R. Landauer, Phys. Rev. B **45**, 1742 (1992).
[37] See Supplementary Material at http://link.aps.org/supplemental/10.1103/PhysRevLett.112.166801 for the data set of a device with $l = 40$ μm.
[38] H. Kamata, N. Kumada, M. Hashisaka, K. Muraki, and T. Fujisawa, Nat. Nanotechnol. **9**, 177 (2014).